Phase separation driven by mobile cations in (Na1−xKx)0.35Co[Fe(CN)6]0.74 zH20

著者	Abe Y., Kim J. E., Matsuda T., Shibata T., Tanida H., Uruga T., Moritomo Y.
journal or publication title	Physical review B
volume	80
number	13
page range	134101
year	2009-10
権利	(C) 2009 The American Physical Society
URL	http://hdl.handle.net/2241/104361

doi: 10.1103/PhysRevB.80.134101

Phase separation driven by mobile cations in $(Na_{1-x}K_x)_{0.35}Co[Fe(CN)_6]_{0.74}\cdot zH_2O$

Y. Abe,[1] J. E. Kim,[2] T. Matsuda,[1] T. Shibata,[1] H. Tanida,[2] T. Uruga,[2] and Y. Moritomo[1,*]
[1]*Graduated School of Pure and Applied Science, University of Tsukuba, Tsukuba 305-8571, Japan*
[2]*JASRI/SPring-8, 1-1-1 Kouto, Sayo-cho, Sayo-gun, Hyogo 679-5198, Japan*
(Received 1 July 2009; revised manuscript received 24 August 2009; published 1 October 2009)

Cation substitution effects on structural and optical properties are investigated for films of Prussian-blue-type cyanides, $(Na_{1-x}K_x)_{0.35}Co[Fe(CN)_6]_{0.74}zH_2O$ $(0.07 \le x \le 0.85)$. Substitution of K^+ for Na^+ induces a phase transition from high-spin (HS) phase with the electronic configuration of $Co^{2+}(t_{2g}^5e_g^2)$-$Fe^{3+}(t_{2g}^5)$ to low-spin (LS) phase with the electronic configuration of $Co^{3+}(t_{2g}^6)$-$Fe^{2+}(t_{2g}^6)$. At around room temperature, the HS phase (LS phase) is observed in the region of $x \le 0.2$ $(x \ge 0.8)$ while two phases coexist in the intermediate-x region $(0.2 \le x \le 0.8)$. We interpreted the two-phase region in terms of *intrinsic* phase separation into small-x (Na^+-rich) and large-x (K^+-rich) regions because the cations can migrate within the crystal to minimize the total free energy. We further confirmed that absorption spectra in the infrared, visible and Co/Fe K edge regions are quantitatively reproduced by the phase-separation model.

DOI: 10.1103/PhysRevB.80.134101 PACS number(s): 64.75.Nx, 61.05.cp, 64.70.K−

I. INTRODUCTION

Phase separation phenomenon is frequently observed in binary alloy and polymer alloy systems, in which total free energy $F(X)$ as a function of order parameter X, e.g., chemical composition, has a common tangent at two values.[1] In this context, the phase separation is possible in hole-doped strongly correlated oxide systems, in which the order parameter is the electron density.[2] Especially, in perovskite-type doped manganites, a colossal magnetoresistive (CMR) effect is enhanced near phase boundary between ferromagnetic metallic and charge-ordered insulating phases, where the phase-separation effect is also enhanced.[3] So far, many researchers experimentally[4–11] and theoretically[12,13] investigated the system to clarify the relation between the phase separation and the CMR effect. However, origin of the phase separation in doped manganites is still controversial because violation of the local charge neutrality causes significant loss of the electrostatic energy.

The hole doping is also possible in Prussian-blue-type cyanides, $A_xM[Fe(CN)_6]_yzH_2O$ (A and M are an alkaline metal and a transition metal, respectively).[14–16] Crystallographically, the compounds belong to the face-centered cubic ($Fm\bar{3}m$;Z=4), in which M and Fe form a rock-salt-type (NaCl-type) network with sharing cyano (CN^-) moieties, -CN-M-NC-Fe-CN-M-.[17] The alkaline metal ions (A^+) and part of water molecules (zeolite water) occupy the nanospaces of the network. Other part of water molecules (ligand water) occupy the $[Fe(CN)_6]$ vacancy and coordinate to the transition metal M. Cation concentration (x), and hence the hole-doping level of the d-electron system, can be controlled by an electrochemical method[18,19] at room temperature. We emphasize that the mobile cation can keep the local charge neutrality, making a sharp contrast with the oxide system. Actually, Moritomo *et al.*[20] reported doping-induced structural phase transition in films of $Na_{1.6-x}Co[Fe(CN)_6]_{0.90}2.9H_2O$ from Rhombohedral phase ($x \le 0.02$) to cubic phase ($x \ge 0.14$). They found that the two lattice structures coexist in the intermediate-x region ($0.02 \le x \le 0.14$) and interpreted the two-phase region in terms of the *intrinsic* phase separation into large-x (Na^+-poor) and small-x (Na^+-rich) regions.

Among the cyanide system, the Co-Fe cyanide is attracting increasing interest of materials scientists because two electronic phases, the high-spin (HS) phase with the electronic configuration of $Co^{2+}(t_{2g}^5e_g^2)$-$Fe^{3+}(t_{2g}^5)$ and the low-spin (LS) phase with the electronic configuration of $Co^{3+}(t_{2g}^6)$-$Fe^{2+}(t_{2g}^6)$, compete with each other. Reflecting larger ionic radius of the HS Co^{2+} [=0.745 Å (Ref. 21)], lattice constant a is much larger (≈10.3 Å) of the HS phase than that (≈9.9 Å) of the LS phase.[22] The two electronic phases can be switched by external stimuli, such as temperature,[22] photoexcitation,[23] reduced pressure,[24] hydrostatic pressure,[25] and cation exchange.[19] Especially, Sato *et al.*[19] reported that substitution of K^+ for Na^+ induces a phase transition from the HS phase to the LS phase. In a naive structural discussion based on the ionic radius, this behavior is curious because substitution of the larger K^+ for the smaller Na^+ should stabilize the HS phase with larger a value.

In this paper, we report structural phase diagram of $(Na_{1-x}K_x)_{0.35}Co[Fe(CN)_6]_{0.74}zH_2O$ as a function of temperature (T) and K^+ concentration (x). The T-x phase diagram indicates that two phases coexist in a wide x region ($0.2 \le x \le 0.8$) around room temperature. We interpreted the two-phase region in terms of the *intrinsic* phase separation into the small-x (Na^+-rich) and the large-x (K^+-rich) regions. We further confirmed that absorption spectra in the infrared, visible, and Co/Fe K edge regions are quantitatively reproduced by the phase-separation model.

II. EXPERIMENT

A. Sample preparation and characterization

The films of $(Na_{1-x}K_x)_{0.35}Co[Fe(CN)_6]_{0.74}zH_2O$ were electrochemically synthesized on an indium tin oxide (ITO) transparent electrodes (sheet resistance was 100 Ω) under potentiostatic condition in an aqueous solution containing 0.5 mmol/L $K_3[Fe(CN)_6]$, 1.25 mmol/L $Co(NO_3)_2$, and 1

TABLE I. Relative concentrations, $\frac{[Na]}{[Co]}$, $\frac{[K]}{[Co]}$, and $\frac{[Fe]}{[Co]}$, of metal elements in Na-K-Co-$[Fe(CN)_6]$-H_2O films as a function of $x_s(\equiv\frac{[K]}{[K]+[Na]})$ of dipping solution. The relative concentrations were determined by an ICP method. Chemical formula of the films can be expressed as $(Na_{1-x}K_x)_{0.35}Co[Fe(CN)_6]_{0.74}zH_2O$.

x_s	$\frac{[Na]}{[Co]}$	$\frac{[K]}{[Co]}$	$\frac{[Fe]}{[Co]}$	$\frac{[Na]+[K]}{[Co]}$	$x\equiv\frac{[K]}{[K]+[Na]}$
0.0	0.328	0.026	0.770	0.356	0.073
0.2	0.202	0.116	0.725	0.318	0.365
0.4	0.178	0.178	0.755	0.356	0.500
0.6	0.131	0.216	0.734	0.347	0.579
0.8	0.105	0.268	0.717	0.373	0.718
1.0	0.053	0.300	0.741	0.353	0.850
average			0.740	0.350	

mol/L $Na(NO_3)$. The thickness ($\approx$1000 nm) of the film was determined by the interference pattern in the infrared-absorption spectrum. Then, the films were oxidized at 0.6 V versus a standard Ag/AgCl electrode in 1 mol $Na(NO_3)$ aqueous solution. The K^+ concentration (x) was controlled by dipping of the film in an aqueous solution containing 1-x_s mol/L NaCl and x_s mol/L KCl for 90 s.

The relative concentrations, $\frac{[Na]}{[Co]}$, $\frac{[K]}{[Co]}$, and $\frac{[Fe]}{[Co]}$, of the metal elements were determined by an inductively coupled plasma (ICP) method (see Table I). As seen in the Table I, magnitudes of $\frac{[Fe]}{[Co]}$(=0.74) and $\frac{[Na]+[K]}{[Co]}$(=0.35) are almost constant, and hence chemical formula of the films can be expressed as $(Na_{1-x}K_x)_{0.35}Co[Fe(CN)_6]_{0.74}zH_2O$. In Fig. 1, we plotted K^+ concentration (x) in film against that (x_s) in the dipping solution. The magnitude of x systematically increases with x_s. We further determined water concentration (z) with use of a carbon-nitrogen-hydrogen (CNH) organic elementary analyzer (Perkin-Elmer 2400 CNH Elemental Analyzer): z=3.65 at x=0.07 and z=2.92 at x=0.85.

In Fig. 2 we show infrared-absorption spectra $\alpha(\hbar\omega)$ for $(Na_{1-x}K_x)_{0.35}Co[Fe(CN)_6]_{0.74}zH_2O$ film at 300 K. The $\alpha(\hbar\omega)$ spectra were measured with use of an infrared microscope system (JASCO IRT-3000) equipped with a Fourier-transform-type infrared spectrometer. The transmitted light was focused on a cooled HgCdTe infrared detector. The absorption band observed at 2160 cm^{-1} for the x=0.07 film is ascribed to the CN stretching mode of the $[Fe(CN)_6]^{3-}$ unit in the HS phase.[14,22] The weak absorption band observed at 2080 cm^{-1} is due to the CN stretching mode of the residual $[Fe(CN)_6]^{4-}$ unit. On the other hand, an intense absorption band observed at 2120 cm^{-1} for the x=0.85 film is due to the CN stretching mode of the $[Fe(CN)_6]^{4-}$ unit in the LS phase.[14,22] Thus, substitution of K^+ for Na^+ induces a phase transition from the HS phase to the LS phase.

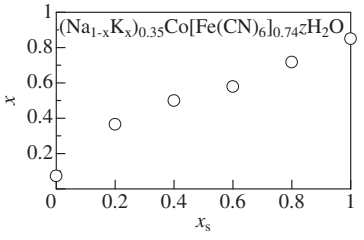

FIG. 1. Relation between K^+ concentration (x) in $(Na_{1-x}K_x)_{0.35}Co[Fe(CN)_6]_{0.74}zH_2O$ films and that ($x_s\equiv\frac{[K]}{[K]+[Na]}$) in dipping solution.

B. Synchrotron radiation x-ray powder diffraction

In order to investigate the structural properties of the films, x-ray powder-diffraction patterns were measured at the synchrotron-radiation facility, SPring-8. First, the film was carefully removed from the ITO glass with a microspatula and then the fine samples were filled into a 300 $\mu m\phi$ glass capillary. The capillary was sealed up and was put on a Debye-Scherrer camera at the BL02B2 beamline[26] of SPring-8. The powder-diffraction pattern was detected with an imaging plate (IP). The exposure time of the IP was 5 min. Wavelength of the x-ray was 0.50279 Å. The sample temperature was controlled with a cooled nitrogen gas in the temperature range of 100 $K\leq T\leq 300$ K. All the films investigated belong to the face-centered cubic ($Fm\bar{3}m$;Z=4).

C. X-ray absorption measurement

The x-ray absorption near edge structure (XANES) were investigated at the synchrotron-radiation facility, SPring-8. The measurements were carried out at 300 K at a broad energy-band beamline BL01B1.[27] XANES near the Co and

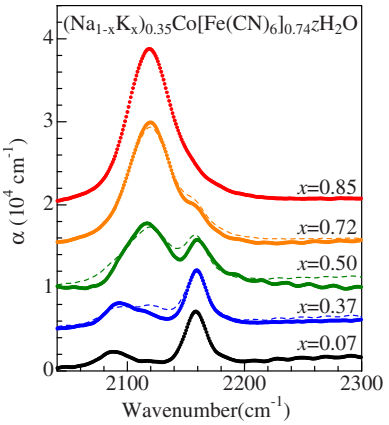

FIG. 2. (Color online) Infrared absorption spectra $\alpha(\hbar\omega)$ for $(Na_{1-x}K_x)_{0.35}Co[Fe(CN)_6]_{0.74}zH_2O$ film at 300 K. Broken curves at x=0.37, 0.58, and 0.72 are the fitting based on the phase-separation model (see text).

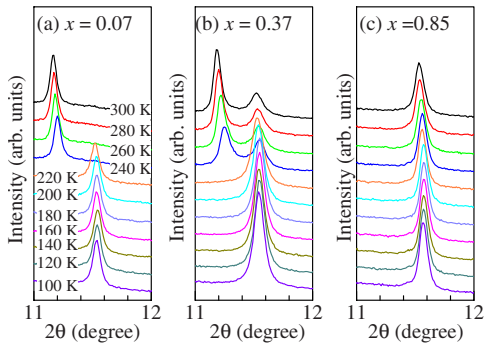

FIG. 3. (Color online) Temperature dependence of magnified diffraction pattern for $(Na_{1-x}K_x)_{0.35}Co[Fe(CN)_6]_{0.74}zH_2O$: (a) $x=0.07$, (b) $x=0.37$, and (c) $x=0.85$. Wavelength of the x ray is 0.50279 Å. Measurements were performed in the cooling run.

Fe K edge were recorded by a Lytle detector in a fluorescent yield mode with a Si(111) double-crystal monochromator. We adopted a quick-scan method, which enables us to obtain each spectrum in 5 min.

III. RESULTS

A. Structural properties

We show in Fig. 3 temperature dependence of magnified diffraction pattern for $(Na_{1-x}K_x)_{0.35}Co[Fe(CN)_6]_{0.74}zH_2O$ film at various x. The observed peak can be indexed as (400) reflection in the face-centered-cubic setting. The small-x film [(a) $x=0.07$] is in the HS phase at 300 K while the large-x film [(c) $x=0.85$] is in the LS phase at 300 K. With decrease in temperature, the scattering angle 2θ of the small-x film (a) discontinuously increases from $\approx 11.2°$ to $\approx 11.6°$ at 230 K. This structural change corresponds to the thermally induced phase transition from the HS phase ($a \approx 10.34$ Å) to the LS phase ($a \approx 10.00$ Å). No structural change is observed for the large-x film (c), indicating that the film remains in the LS phase ($a \approx 10.00$ Å). A rather complicated behavior is observed for the intermediate-x film [(b) $x=0.37$]: two reflections are observed above 230 K while the lower-lying peak disappears below 230 K. The two-peak feature above 230 K is ascribed to coexistence of the HS phase and the LS phase. Actually, overall diffraction pattern at 300 K is well reproduced by the Rietveld refinement with the two-phase model (see Table II). Hereafter, we call this phase-separated state as "HS+LS" phase. We emphasize that the width of the reflection below 230 K is as sharp as that of the large-x film (c), indicating that the film is in the single LS phase below 230 K.

We determined magnitudes of a by the Rietveld analysis and plotted them as a function of temperature in Fig. 4. The small-x film [(a) $x=0.07$] shows a phase transition from the HS phase ($a \approx 10.3$ Å) to the LS phase ($a \approx 10.0$ Å). On the other hand, the large-x film [(c) $x=0.85$] is in the LS phase ($a \approx 10.0$ Å) in the temperature range investigated. In the intermediate-x sample [(b) $x=0.36$], a structural transition from the HS+LS phase ($T \geq 230$ K) to the LS phase ($T \leq 230$ K) is observed. Interestingly enough, a of the LS phase shows a slight jump at 230 K [see closed circles in Fig. 4(b)]. This indicates that something, e.g., chemical composition, is different between the low-temperature LS phase and the high-temperature LS phase.

TABLE II. Lattice constant a and mass fraction s of the LS phase in $(Na_{1-x}K_x)_{0.35}Co[Fe(CN)_6]_{0.74}zH_2O$ at 300 K. a and s were determined by Rietveld analysis. HS and LS represent high-spin phase and low-spin phase, respectively. Reliable parameter $R_{wp}(\equiv[\frac{\Sigma_i w_i(y_i-y_{i,calc})^2}{\Sigma_i w_i y_i^2}]^{1/2})$ is also listed.

	HS	LS		
x	a (Å)	a (Å)	s	R_{wp}
0.07	10.3414(3)		0	2.52%
0.37	10.3230(3)	10.0180(8)	0.37	3.87%
0.50	10.3145(5)	10.0056(8)	0.43	2.43%
0.72	10.3061(5)	10.0039(3)	0.77	6.14%
0.85		10.0102(3)	1	3.44%

We summarized in Fig. 5(a) structural phase diagram for $(Na_{1-x}K_x)_{0.35}Co[Fe(CN)_6]_{0.74}zH_2O$ against x The HS phase (LS phase) is observed in the region of $x \leq 0.2$ ($x \geq 0.8$) at around 300 K while the HS+LS phase appears in the intermediate-x region ($0.2 \leq x \leq 0.8$). With decrease in temperature, both the HS phase and the HS+LS phase change into the LS phase. In Figs. 5(b) and 5(c), we plot lattice parameters, a and mass fraction s of the LS phase. Looking at Fig. 5(b), one may notice that magnitude of a in the HS phase slightly decreases with x. This is perhaps due to decrease in the water concentration (z): $z=3.65$ at $x=0.07$ and $z=2.92$ at $x=0.85$. Magnitude of s linearly increases with x, as indicated by the least-square-fitted straight line in Fig. 5(c).

These structural features are well understood by a phase-separation model.[1] Looking at the phase diagram [Fig. 5(a)], one may notice that the HS is stable in the small-x region while the LS phase is stable in the large-x region. Then, the total free energy $F(x)$ is considered to have a common tangent at two doping levels, $x_{HS}(\sim 0)$ and $x_{LS}(\sim 1)$. With such a $F(x)$ profile, the cations migrate so as to create Na^+-rich (x

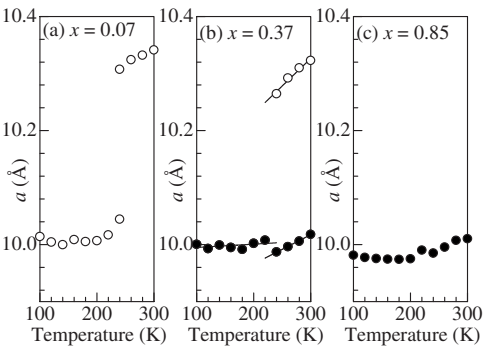

FIG. 4. Temperature dependence of lattice constant a for $(Na_{1-x}K_x)_{0.35}Co[Fe(CN)_6]_{0.74}zH_2O$: (a) $x=0.07$, (b) $x=0.37$, and (c) $x=0.85$. Open (closed) circles represent the HS (LS) phase. Magnitude of a was determined by Rietveld refinement. Straight line in (b) is results of the least-square fitting.

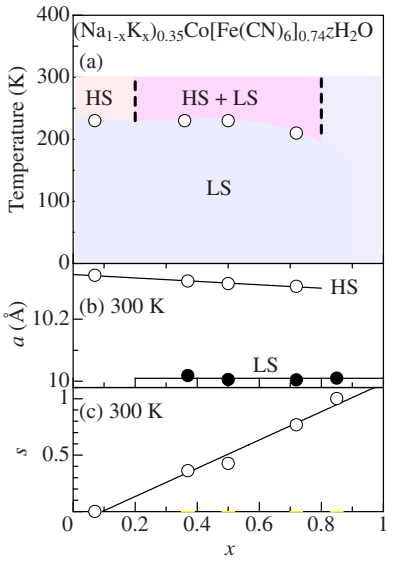

FIG. 5. (Color online) (a) Structural phase diagram for $(Na_{1-x}K_x)_{0.35}Co[Fe(CN)_6]_{0.74}zH_2O$ against x. HS and LS represent high-spin phase and low-spin phase, respectively. (b) Lattice constant a of the HS phase (open circles) and the LS phase (closed circles) at 300 K. (c) Mass fraction s of the LS phase at 300 K. Straight lines in (bright) and (c) are results of the least-square fitting.

$=x_{HS}$) and K^+-rich ($x=x_{LS}$) regions. The $x=x_{HS}$ (x_{LS}) region becomes the HS phase (LS) phase. Within this scenario, we obtain an interrelation between s and x: $s=\frac{x-x_{HS}}{x_{LS}-x_{HS}}$. This equation well explains experimentally obtained s-x curve [Fig. 5(b)]. In this phase-separation scenario, the slight jump of a observed at $x=0.37$ [see Fig. 4(b)] can be ascribed to the different local K^+ concentration x_{local}: $x_{local}=x$ for the low-temperature LS phase and $x_{local}=x_{LS}$ for the high-temperature LS phase.

B. Visible and infrared-absorption spectra

Figure 6 shows the visible absorption spectra $\alpha(\hbar\omega)$ for $(Na_{1-x}K_x)_{0.35}Co[Fe(CN)_6]_{0.74}zH_2O$ film at 300 K. $\alpha(\hbar\omega)$

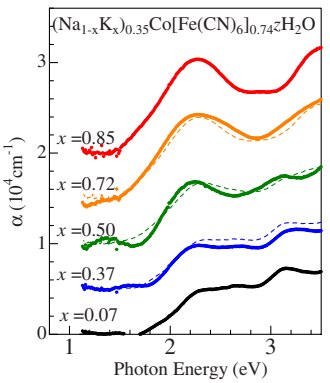

FIG. 6. (Color online) Visible absorption spectra $\alpha(\hbar\omega)$ for $(Na_{1-x}K_x)_{0.35}Co[Fe(CN)_6]_{0.74}zH_2O$ film at 300 K. Broken curves at $x=0.37$, 0.58, and 0.72 are the fitting based on the phase-separation model (see text).

TABLE III. Fractions, s, s', and s'', of the LS phase for $(Na_{1-x}K_x)_{0.35}Co[Fe(CN)_6]_{0.74}zH_2O$ film. s was determined by Rietveld analysis with two-phase model. s' was determined by the fitting of absorption spectra in the infrared and visible regions. s'' was determined by the fitting of x-ray absorption spectra.

x	s	s'	s''
0.37	0.37	0.10	0.37
0.50	0.43	0.35	0.40
0.72	0.77	0.75	0.75

spectra were measured with a conventional monochromator system with an Xeon lamp. The transmitted light was focused on a Si photodiode and a lock-in detection was adopted to enhance the S/N ratio. The absorption edge for the $x=0.07$ film (HS phase) is assigned to charge-transfer (CT) transition from the Co^{2+} site to the Fe^{3+} site.[14,22] The absorption edge for the $x=0.85$ film (LS phase) is assigned to CT transition from the Fe^{2+} site to the Co^{3+} site.[16,22]

Here, let us analyze the $\alpha(\hbar\omega)$ spectra in the intermediate-x region within the phase-separation model. If the phase-separated domain is comparable to, or larger than, the wavelength of probe light, the effective absorption coefficient $\alpha_x(\hbar\omega)$ at x is the spatial average of the local absorption coefficient. Then, $\alpha_x(\hbar\omega)$ can be expressed as

$$\alpha_x(\hbar\omega) = (1-s')\alpha_{HS}(\hbar\omega) + s'\alpha_{LS}(\hbar\omega), \quad (1)$$

where s' is fraction of the LS phase. We regarded the $\alpha_{x=0.07}(\hbar\omega)[\alpha_{x=0.85}(\hbar\omega)]$ spectrum as the $\alpha_{HS}(\hbar\omega)[\alpha_{LS}(\hbar\omega)]$ spectrum. Broken curved in Fig. 6 are the best-fitted results: $s'=0.10$ at $x=0.37$, $s'=0.35$ at $x=0.50$ and $s'=0.75$ at $x=0.72$. We further applied the same analysis to the infrared-absorption spectra with the same set of s'-values. The phase-separation model with single fitting parameter (s') quantitatively reproduces the absorption spectra in both the infrared (Fig. 2) and visible (Fig. 6) regions.

In Table III, we compare magnitudes of the structurally determined fraction (s) and that of the spectroscopically determined fraction (s'). Agreement between them is satisfactory except for the $x=0.37$ film. We suspect smallness of the domain size causes the discrepancy at $x=0.37$. Actually, we obtained a more excellent agreement between s and that (s'') determined by the x-ray absorption spectra, as described in the Sec. III C. Here note that the wavelength of an x ray is order of the interatomic distance, and hence, the x-ray absorption phenomenon is free from the domain-size effect.

C. x-ray absorption spectra

Figure 7 shows the x-ray absorption spectra near (a) Co K edge and (b) Fe K edge for $(Na_{1-x}K_x)_{0.35}Co[Fe(CN)_6]_{0.74}zH_2O$ film at 300 K. The Co K edge (Fe K edge) spectra were normalized by the local maxima around 7744 eV (7146 eV). The Co K edge spectra in Fig. 7(a) shows significant x dependence. 7723 eV peak observed at $x=0.07$ is ascribed to the HS Co^{2+} ions while 7727 eV peak observed at $x=0.85$ is due to the LS Co^{3+} ions.[28] Intensity of the 7723 eV peak gradually decreases

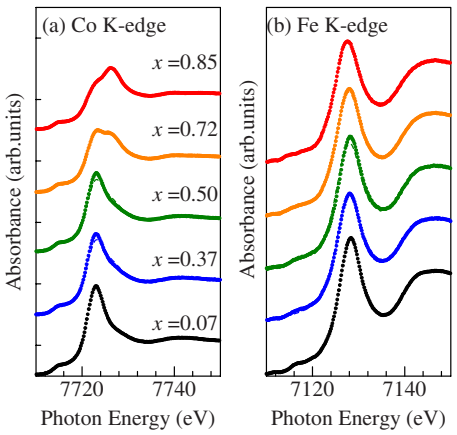

FIG. 7. (Color online) X-ray absorption spectra near (a) Co *K* edge and (b) Fe *K* edge for $(Na_{1-x}K_x)_{0.35}Co[Fe(CN)_6]_{0.74}zH_2O$ film at 300 K. Broken curves at $x=0.37$, 0.58, and 0.72 are the fitting based on the phase-separation model (see text).

with x. Nevertheless, trace of the peak is discernible even at $x=0.85$, indicating that part of the Co sites remains to be divalent even in the LS phase. This observation is consistent with the extended chemical formula of the respective phases: $(Na^{I}_{1-x}K^{I}_{x})_{0.35}Co^{II}_{0.39}Co^{III}_{0.61}[Fe^{II}(CN)_6]_{0.74}zH_2O$ in the LS phase and $(Na^{I}_{1-x}K^{I}_{x})_{0.35}Co^{II}[Fe^{III}(CN)_6]_{0.61}[Fe^{II}(CN)_6]_{0.13}zH_2O$ in the HS phase. The formulas indicate that 39% Co site remains divalent in the LS phase while all the Co sites become divalent in the HS phase. On the other hand, the Fe *K* edge spectra in Fig. 7(b) shows negligible change except for slight redshift ($\approx$0.8 eV) with increase in x.

We applied the phase-separation model to the x-ray absorption spectra

$$\alpha_x(\hbar\omega) = (1 - s'')\alpha_{HS}(\hbar\omega) + s''\alpha_{LS}(\hbar\omega), \qquad (2)$$

where s'' is fraction of the LS phase. We regarded the $\alpha_{x=0.07}(\hbar\omega)$ $[\alpha_{x=0.85}(\hbar\omega)]$ spectrum as the $\alpha_{HS}(\hbar\omega)$ $[\alpha_{LS}(\hbar\omega)]$ spectrum. Broken curved in Fig. 7 are the best-fitted results: $s''=0.37$ at $x=0.37$, $s''=0.40$ at $x=0.50$, and $s''=0.75$ at $x=0.72$. In Table III, we compare magnitudes of s and s''. Agreement between them is excellent.

IV. DISCUSSION

Finally, let us discuss the origin of the stabilization of the LS phase in the K^+-substituted compound [see Fig. 5(a)]. We emphasize that a naive structural discussion based on the ionic radius fails to explain the K^+-substitution effect. Because ionic radius (=1.51 Å) of K^+ is much larger than that (=1.18 Å) of Na^+ and hence the K^+ doping is expected to stabilize the HS phase with larger unit-cell volume.

The magnitude of the ligand field ($10Dq$) around the Co site is a key parameter that governs the stability of the LS phase. Actually, Shimamoto *et al.*[22] investigated the interrelation between the stability of the LS phase and the concentration (y) of $[Fe(CN)_6]$, and found that the LS phase is stabilized with increase in y via the enhanced ligand field. In addition, Moritomo *et al.*[24] investigated the reduced pressure effects on the critical temperature T_c for the HS $-$LS phase transition and found that the removal of the zeolite water stabilizes the LS phase. This phenomenon was ascribed to the volume compression effect, which also enhances the ligand field. In the present solid solution $(Na_{1-x}K_x)_{0.35}Co[Fe(CN)_6]_{0.74}zH_2O$, the water concentration z decreases from $z=3.65$ at $x=0.07$ (K compound) to $z=2.92$ at $x=0.85$ (Na compound). Such a reduction in z causes the volume compression in both the HS and LS phases, as observed in Fig. 5(b). Thus, the stabilization of the LS phase by the K^+ doping can be ascribed to removal of the zeolite waters and resultant volume compression.

V. SUMMARY

In summary, we systematically investigated lattice structure of $(Na_{1-x}K_x)_{0.35}Co[Fe(CN)_6]_{0.74}zH_2O$ as a function of temperature (T) and K^+ concentration (x), and determined $T-x$ structural phase diagram. The phase diagram indicates that the HS phase and the LS phase coexist in a wide x region ($0.2\leq x\leq 0.8$) around room temperature. In the phase-separated region, magnitudes of the structurally determined fraction s of the LS phase agree with those of the spectroscopically determined fraction, s' and s''. We ascribed the stabilization of the LS phase by the K^+ doping to removal of the zeolite water and resultant volume compression.

ACKNOWLEDGMENTS

This work was supported by a Grant-In-Aid for Scientific Research from the Ministry of Education, Culture, Sports, Science and Technology. The synchrotron-radiation x-ray powder-diffraction experiments were performed at the SPring-8 BL02B2 beamline with approval of the Japan Synchrotron Radiation Research Institute (JASRI). The x-ray absorption near-edge structure measurements were performed at the SPring-8 BL01B1 beamline with approval of JASRI. We are grateful to H. Oosawa for his help in the XANES experiment. Elementary analysis of the films was performed at Chemical Analysis Division, Research Facility Center for Science and Engineering, University of Tsukuba.

*Author to whom correspondence should be addressed.

[1] C. Kittel and H. Kroemer, *Thermal Physics*, 2nd ed. (W. H. Freeman and Company, New York, 1980).

[2] M. Yu. Kagan, D. I. Khomskii, and M. V. Mostovoy, Eur. Phys. J. B **12**, 217 (1999).

[3] Y. Moritomo, Phys. Rev. B **60**, 10374 (1999).

[4] A. Machida, Y. Moritomo, E. Nishibori, M. Takata, M. Sakata, K. Ohoyama, S. Mori, N. Yamamoto, and A. Nakamura, Phys. Rev. B **62**, 3883 (2000).

[5] M. Uehara, S. Mori, C. H. Chen, and S.-W. Cheong, Nature

(London) **399**, 560 (1999).
[6] P. Schiffer, A. P. Ramirez, W. Bao, and S.-W. Cheong, Phys. Rev. Lett. **75**, 3336 (1995).
[7] S. Mori, C.-H. Chen, and S.-W. Cheong, Phys. Rev. Lett. **81**, 3972 (1998).
[8] G. Allodi, R. De Renzi, F. Licci, and M. W. Pieper, Phys. Rev. Lett. **81**, 4736 (1998).
[9] G. Papavassiliou, M. Fardis, M. Belesi, T. G. Maris, G. Kallias, M. Pissas, D. Niarchos, C. Dimitropoulos, and J. Dolinsek, Phys. Rev. Lett. **84**, 761 (2000).
[10] P. G. Radaelli, D. E. Cox, M. Marezio, S.-W. Cheong, P. E. Schiffer, and A. P. Ramirez, Phys. Rev. Lett. **75**, 4488 (1995).
[11] M. Jaime, P. Lin, S. H. Chun, M. B. Salamon, P. Dorsey, and M. Rubinstein, Phys. Rev. B **60**, 1028 (1999).
[12] S. Yunoki, J. Hu, A. L. Malvezzi, A. Moreo, N. Furukawa, and E. Dagotto, Phys. Rev. Lett. **80**, 845 (1998).
[13] S. Okamoto, S. Ishihara, and S. Maekawa, Phys. Rev. B **61**, 451 (2000).
[14] F. Nakada, H. Kamioka, Y. Moritomo, J. E. Kim, and M. Takata, Phys. Rev. B **77**, 224436 (2008).
[15] T. Shibata, F. Nakada, H. Kamioka, and Y. Moritomo, J. Phys. Soc. Jpn. **77**, 104714 (2008).
[16] K. Igarashi, F. Nakada, and Y. Moritomo, Phys. Rev. B **78**, 235106 (2008).
[17] H. J. Buser, D. Schwarzenbach, W. Petter, and A. Ludi, Inorg. Chem. **16**, 2704 (1977).
[18] K. Itaya, I. Uchida, and D. V. Neff, Acc. Chem. Res. **19**, 162 (1986).
[19] O. Sato, Y. Einaga, T. Iyoda, A. Fujishima, and K. Hashimoto, J. Phys. Chem. B **101**, 3903 (1997).
[20] Y. Moritomo, K. Igarashi, T. Matsuda, and J. E. Kim, J. Phys. Soc. Jpn. **78**, 074602 (2009).
[21] R. D. Shannon, Acta Crystallogr. A **32**, 751 (1976).
[22] N. Shimamoto, S. Ohkoshi, O. Sato, and K. Hashimoto, Inorg. Chem. **41**, 678 (2002).
[23] O. Sato, T. Iyoda, A. Fujishima, and K. Hashimoto, Science **272**, 704 (1996).
[24] Y. Moritomo, F. Nakada, J. E. Kim, and M. Takata, Appl. Phys. Express **1**, 111301 (2008).
[25] M. Hanawa, Y. Moritomo, J. Tateichi, Y. Ohishi, and K. Kato, J. Phys. Soc. Jpn. **73**, 2759 (2004).
[26] E. Nishibori, M. Takata, K. Kato, M. Sakata, Y. Kubota, S. Aoyagi, Y. Kuroiwa, M. Yamakawa, and N. Ikeda, Nucl. Instrum. Methods Phys. Res. A **467-468**, 1045 (2001).
[27] T. Uruga, H. Tanida, Y. Yoneda, K. Takeshita, S. Emura, M. Takahashi, M. Harada, Y. Nishihata, Y. Kubozono, T. Tanaka, T. Yamamoto, H. Maeda, O. Kamishima, Y. Takabayashi, Y. Nakata, H. Kimura, S. Goto, and T. Ishikawa, J. Synchrotron Radiat. **6**, 143 (1999).
[28] T. Yokoyama, T. Ohta, O. Sato, and K. Hashimoto, Phys. Rev. B **58**, 8257 (1998).